DOI: https://doi.org/10.24297/ijct.v22i.9228

Hyalite Sol-Gel Amoeba: A Physiology-Based Biophysical Model for Segmentation and Biotransformation of Medical Images To 3D Solid-State Characterizing Native Tissue Properties for Patient-Specific and Patient-Appropriate Analysis for Surgical Applications

Gandhi, Harjeet Singh MD, FRCS, FRCSC, MSc (Biomed Eng.)

Orthopaedic surgeon, Clinical Assistant, Hamilton Health Sciences, Hamilton, Ontario, Canada

harjeetg52@yahoo.co.uk

Abstract

Introduction: The endeavour to improve medical image segmentation techniques for higher analysis in surgical planning and medical therapeutics is far from becoming a standard of care in clinical practice. Hyalite Sol-Gel Amoeba model based on biophysical sciences apart from performing image segmentation is designed to extract real-world tissue densities for patient-specific and patient-appropriate analysis.

Objectives: Amoeba Proteus is a unicellular independent entity, with a nucleus and sol-gel protoplasm enclosed in a membrane. The study presents versatile restructuring anatomy and physiology of the Amoeba Proteus for segmentation of 2D, and 3D medical images based on well-established principles of energy minimization and active contour. It demonstrates how the animalcule glides and advances by throwing pseudopodia driven by phenomenal actin-myosin activity that can segment a region-of-interest, and finally, at the time of apoptosis, its protoplasm and organelles acquire distribution of original image intensities to characterize tissue densities.

Methods: This seminal study following a brief review of computer vision science discusses the relationship between optical density and tissue density, and the theory of sol-gel fluid mechanics. The theoretical framework of the HSG-Amoeba is described with the segmentation of various skeletal components of the thoracic cage.

Results: This being a foundational study to describe the concept of the HSG-Amoeba model it requires the development of a mathematical algorithm to demonstrate its worthiness as a tool for surgical applications.

Conclusion: The focus of the study is to present the design and framework of the newly conceived HSG-Amoeba model to segment a medical image and extract tissue densities without altering the original image intensities.

Keywords: Sternotomy, osteochondrotomy, intensiotaxis, intensiokinesis, optical density, tissue density, computer vision, clinical biomechanical engineer

Short title: Hyalite sol-gel Amoeba: A physiology-based biophysical model

1.0 Background

The purpose of processing medical images is to perform higher-level [1]*patient-specific* and *patient-appropriate*(Gandhi, 2019) systematic evaluations. For surgical applications, the best available method is finite element analysis by constructing a finite element model of a segmented region-of-interest (R-O-I). Although there are numerous well-known segmentation methods for industrial and medical applications, however, unlike homogeneous industrial images the medical images are unique being heterogeneous due to variable tissue densities and extracellular body fluids, and noise related to imaging instruments that result in a wide range of nuisance pixel grey-level values. The segmentation of medical images is undertaken to study either normal regional anatomy or isolate a disease-specific zone in an R-O-I to examine the progression of tissue pathology during follow-up and/or develop treatment strategies. Currently, none of the available segmentation techniques provide information about the real native tissue densities as a function of original representative pixel grey-level values to derive mechanical properties thereof for higher mathematical analysis. The study describes the

[1] Foot note: The word *'specific'* refers to a precise anatomical location or an entire segment of a region or organ system, e.g., head of the humerus of the skeletal system, and *'appropriate'* means that something is suitable and favourable only for a single patient under special circumstances, including patient physique and multiple influential co-morbidities. A technique can only be called *'patient-specific'* if the collected set of data to which it is applied belongs to a specific anatomical section/segment of a bone as in the case of skeleton or a specific element of an organ for biomechanical evaluation and higher numerical analysis for clinical application rather than to the entire organ system of that individual. More importantly, it is done without the inclusion of any kind of extraneous experimental or population based statistical values to constitute *"patient-appropriate medicine."*

biomimetic mechanisms of the proposed hyalite sol-gel Amoeba (HSG-Amoeba) model for the segmentation of medical images to finally extract tissue densities based on each pixel grey-level value and calculate elastic modulus using one of the known power laws for finite element analysis and select an implant to reconstruct the anatomy of a bone. In addition, it reviews related computer vision science and the relevance of optical density to elucidate the distribution of representative tissue densities in an image.

The rationale to prefer Amoeba Proteus as a motif for image segmentation is its dynamic physiological processes such as asexual reproduction, formation of pseudopodia for motility, and alternating sol-gel phases in the cytoplasm that occur at the molecular level. The energy-dependent autonomous function for its motility is based on chemical feedback and external stimulus-response phenomenon that arise from its immediate environment. To reach its energy source and forage the environment precisely based on certain cues the Amoeba Proteus throws out as many pseudopodia as needed. The motion is generated by spontaneous coupling and decoupling of the Actin network in the endoplasm to extend its pseudopodia(Blanchoin et al., 2014; Pollard & Borisy, 2003).

2.0 Pertinent aspects of computer vision

The development of computer vision has become an everyday facultative instrument to facilitate many functions of the human visual system to assist in diagnosis and planning medical treatments. Human vision has a special advantage over computer vision, in that, it can subjectively judge and react to qualitative and quantitative material properties of fluids and solids from their appearance and density without engaging other sensory faculties. From this perspective, the HSG-Amoeba model is a step toward the derivation of material density, hence the mechanical properties of the biological materials that concern the present study within the field of clinical biomechanical engineering and concepts of computer vision.

An image is an optical virtual reality pattern of a real object represented in the form of intensities (multiple levels of brightness) distributed in another space referred to as image space relative to the real-world physical space of a real 2D or 3D object. Any digital image in image space has a minimum of two functional variables – one as its brightness in the form of grey tones or grey-level values and the second as its location in the x and y coordinates of 2D space. For the concept to be clinically valuable the virtual image space must correspond to the real-world physical space for accurate diagnosis and to translate it into pathological anatomy for enhancing the patient management skills of physicians and positioning of instruments for specific operations, whether it is interventional radiology or computer navigated endoscopic surgery.

In an image, the optimal size and number of pixels are important for image resolution, but each pixel does not have significant details except the grey-level value. In processing medical images segmentation and registration are the most primitive activities to define an object or an R-O-I within a busy image like the thorax. Unfortunately, there is no ideal universal segmentation method that can be applied to all kinds of medical images. Automatic segmentation is not picture-perfect due to the variable anatomy and the heterogeneous nature of the medical images, therefore manual interaction with an expert becomes necessary.

Almost all medical digital images are a collection of complete and partial anatomy of organs containing physical properties of various constituting tissues stored as discrete mathematical functions in the form of image data. The imaging modality used must reproduce a true representation of the real-world physical space such that the information provided is meaningful. And the image processing technology for segmentation can transform the subjective biological properties into objective mathematical quantities embedded in the registered image and is ultimately made available for clinical applications. The design of the segmentation algorithm should be such that it can put together information of all pixels within the region-of-interest without ambiguities and in continuity rather than piecewise information fitted together like a patchwork.

In radiology, visual illusions are not uncommon due to the busy physical environment of the image to distract the observers(Buckle et al., 2013). The human visual system can only discriminate around 30 consecutive brightness levels in an image, beyond which the eyes would be unable to distinguish between neighbouring grey tones(GEOFF DOUGHERTY, 2009). An ideal segmentation method to isolate an R-O-I is of greater value than visual isolation by human vision only if the method creates the virtual image space such that it corresponds to the real physical space. At the same time, the designed mathematical algorithm can reverse the inverse R-O-I in the image space to the real-world physical space in the form of quantitative data. So that original tissue

densities and material properties of the imaged biological tissues can be realized as a set of data to carry out higher practical analysis for clinical applications.

Medical images are much more than just foreground and background binary images, being conglomerates of a variety of tissues, overlapping each other without distinct sharp margins between neighbours as there are no empty spaces in the living animal anatomy. The segmentation method should not exclude desirable or include undesirable pixels, particularly when it is applied to a malignant lesion during follow-up and surgical intervention. As there can be progressive changes in the tissue properties in the neighbourhood structures, it should also provide the tissue properties to meet the haptic needs of surgical application during surgical manipulation such as incision, retraction, and resection.

It is an intense exercise to segregate R-O-I within medical images generated by radiation and magnetic resonance modalities that represent remote hidden internal structures with multiple layers of highly heterogeneous tissues. It is like remote sensing military-strategic applications, environment surveillance surrounding autonomous vehicles, and dense woodlands in urban areas to extract accurate information for various applications. In such cases, object-oriented thresholding, edge detection, and statistics-based segmentation techniques are less than ideal compared to machine learning algorithms(Wang et al., 2016). In the case of complex busy and diverse image content deep learning convolutional neural network provides superior results(Saito et al., 2016) and a fully convolutional network with a multilayer convolution network structure with the addition of a de-convolutional layer can segment region-of-interest pixel-by-pixel(Dolz et al., 2018; Jones, 2014).

2.1 Variable tissue densities and image intensities

The biological structures consist of a variety of tissues such as skin, mucosa, and glandular tissues; fibrous and muscular tissues; joint capsule, ligaments, and varying densities of bone depending on site, age, gender, and physical activities. Each of these tissues has different densities and material properties that cause a variable degree of attenuation (reduce by absorption) and scatter of x-ray photons. A varying degree of water content influences the response to the magnetic resonance producing extremely heterogeneous images. Currently, bone density expressed in Hounsfield unit (HU), or computed tomography (CT) number is the average grey-level value of several pixels. The Hounsfield scale in terms of radiodensity is based on a linear relationship to the attenuation coefficient of distilled water equal to zero HU. Generally, bone mineral density (BMD) is calculated by subtracting soft tissue density as a differential between the absorption of two varying energy x-ray beams passing through a composite structure made-up of soft tissues and skeleton. To extract tissue material properties for clinical applications mathematical calculations are undertaken to correlate HU, BMD, bone apparent density, and modulus of elasticity. Bone as seen in an image usually has a density equivalent to or more than 50 Hounsfield units, the air is -1000HU, water 0HU, and normal diaphyseal bone cortex +1000HU(GEOFF DOUGHERTY, 2009). At the time of segmentation, if the threshold chosen is more than 250HU based on the intensity histogram for feature extraction, then any bone with extreme osteoporosis will be intentionally excluded, and no quantitative information about the pathological soft tissues will be included for analysis. A specialized image processing method is needed to provide quantitative tissue properties pixel-by-pixel based on grey-level values and intensity gradient to include all varieties of tissues in the field of interest. Computing piecewise information can be not only time-consuming but too expensive in cases of elective surgery for pre-operative planning. Medical image processing can only be called successful if it provides real-world physical space properties in the form of practical data that can be applied to clinical practice through higher image analysis during treatment planning realizing them into ameliorative therapeutic medical and surgical interventions.

2.2 Role of intensity histogram in processing medical images

An intensity histogram is a statistical representation of the relationship between several pixels in each digital image and the distribution of the grey-level scale on the x, and y coordinates (Haralick, RM. & Shapiro, 1985) (Fig. 1). The distribution of the grey-level values can vary from pixel to pixel or many pixels in an image can share the same grey-level value. This variation is because of the number of photons reflecting from the object to strike the light-sensitive digital sensor plate (photo-site) of the recording modality generating the digital image. When

the appearance of the exposed object has homogeneous surface properties and its surrounding environment also happens to have homogeneous but distinctive properties, then the image will be binary. In that case, the

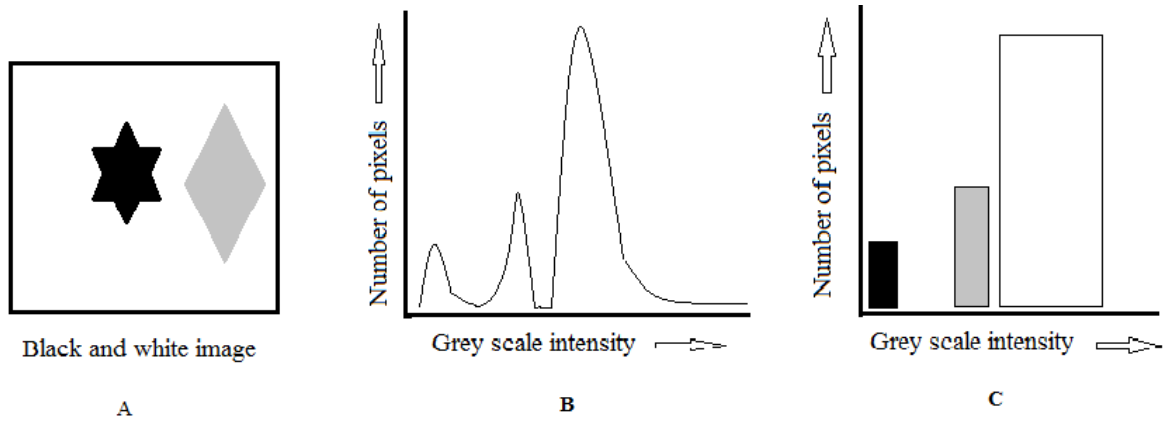

Figure 1 – A. Image of black and white objects; B. Multimodal graphic representation of the greyscale intensities; and C. greyscale intensity histogram of the same image.

intensity histogram will be bi-modal (0 and 1), which is considered useful for segmentation techniques. Other than being a black-and-white image, it does not provide any useful information regarding the nature of the object and its material properties without prior knowledge of the object. The intensity histograms are also the basis for further engineering of the image characteristics during pre-processing for enhancement and equalization of pixel grey-level values by spreading them evenly in each region of the image to increase its spectral value. Such intentional enhancement leads to the loss of original information creating an entirely new image with altered visual and apparent material properties. The equalization process also changes the number of grey-level values, corrupts many important features of the image, and would prevent the extraction of original quantities for higher image analysis. Following pre-processing, the intensity histogram of the new image is used to choose grey-level threshold values for segmentation and further image processing.

Thus, to enhance the image quality the original intensity histogram carrying important mathematical data from the digital image as a discrete function of the grey-level and representative number of pixels is lost forever. This is in addition to the loss of information when the heterogeneous 3D real-world representation of biological tissues is transformed into 2D medical digital images. Therefore, image enhancement is counterproductive in the case of medical images for segmentation when it comes to higher analysis for clinical applications.

As medical images are a record of attenuation due to absorption and dispersion of x-ray photons, so their grey-level values are the best parameters to extract natural values of tissue densities occurring in a patient's physical space. Only true grey-level values representative of heterogeneous tissue densities of internal structures of the body are clinically valuable. To achieve this objective there is a crucial need for further development of imaging modalities and standardization of current technical parameters, such as x-ray beam strength, exposure time, and subject-related parameters.

3.0 Application of optical density principles to tissue density

Optical density is a measure of electromagnetic waves of visible light or ionizing radiation transmitted through an object and registered as brightness on a recording unit. Mathematically, it is a relative measure of numbers, a logarithmic intensity ratio of absorbance and transmittance of an electromagnetic wave through a material, hence without any measurement unit. Therefore, attenuation of the wave as the property of a material on a logarithmic scale is expressed as OpD = $-\log_{10}$ Intensity of incident light / Intensity of transmitted light. In the case of x-ray images, the optical density can be expressed as Tissue attenuation density = $-\log_{10}$ Intensity of incident x-ray beam / Intensity of transmitted x-ray. The optical density of a transparent object is zero if 100% of the wave is transmitted through it. If 10% of light passes through a medium its optical density is 1 and, for 1% and 0.1% the number would be 2 and 3 respectively(GEOFF DOUGHERTY, 2009). Higher optical density materials register darker with relatively little brightness. The higher the exposure to light or x-ray of a light-sensitive film coated with silver halide emulsion darker would be the response. The exposure is the total amount

of incident electromagnetic waves, which is expressed as the product of exposure time and recorded brightness intensity. The particle analog image is different from a digital image. The intensity of the digital image is the function of the quantized pixel grey-level value. A useful logarithmic scale can be developed to relate pixel grey-level scale or intensity gradient and optical density of biological tissues based on the principle of relationship between the optical density of the emulsion concentration and log of relative exposure, as its response in the form of image intensity or brightness.

An advanced-level algorithm can be developed based on the grey-level scale to measure the intensity gradient for matching and extraction of practical information. In forestry and agriculture, colour image analysis is undertaken to quantify chlorophyll in healthy and diseased leaves by using Color Pro© software (Electronic systems division). The software matches and measures the colour intensity of each leaf against an arbitrary colour unit in the form of intensity as the inverse integrated grey-level value per pixel, which is proportional to the actual concentration of chlorophyll per pixel in the image of any leaf generated under standard conditions of illumination(Swaroop & Sharma, 2016). When the 8-bit red, green, and blue colour image is transformed into a grey-level scale there will be more than 16 million colour or grey tones (2^8 x 2^8 x 2^8 = 256^3 = 16,777,216). If the Color Pro© technique is translated to a medical image intensity gradient with heterogeneous distribution of pixel grey-level values representing heterogeneous tissues responsible for variable intensity due to tissue density or concentration of mineral density in the case of bone tissue, it is possible to calculate bone density in each pixel. In various sub-zones of a segmented R-O-I in an image, individual tissue density can be calculated as a product of mineral or protein concentration per pixel and the number of pixels in the zone. In plant biochemistry, Color Pro© software has already been used to estimate the amount of protein in plant materials(Bannur et al., 1999).

3.1 Constructing an intensity-density histogram -

Interestingly, the graphic relationship of optical density (concentration of emulsion) to the logarithm of relative exposure(GEOFF DOUGHERTY, 2009) is like that of pixel intensity grey-level scale to the concentration of chlorophyll in leaves. The quantity of chlorophyll in the leaves responsible for its optical density is like the amount of collagen proteins and calcium responsible for image intensity representing bone density. Hence, for

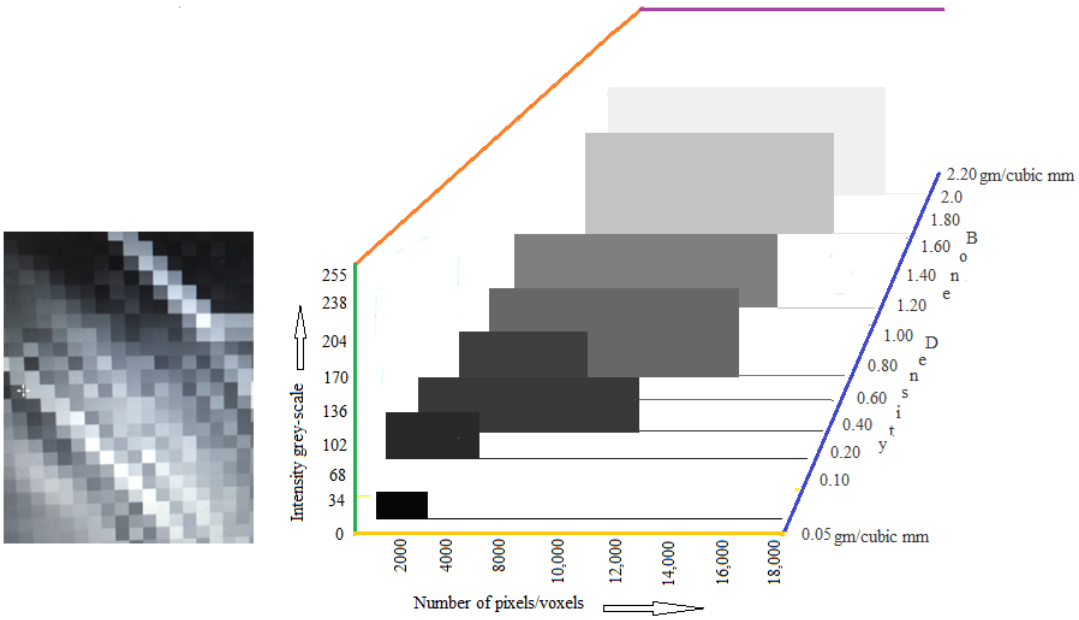

Figure 2 – Three-dimensional histogram showing the relationship between intensity grey-scale and likely bone density, accompanying a symbolic raster image.

estimation of tissue density and material properties thereof, the hypothetical algorithm flow can be - *Input medical image → optical density/pixel intensity value reader → pixel intensity value converter to Hounsfield unit → output image tissue density distribution record from Hounsfield unit → tissue density to tissue material property converter*. The tissue-specific material properties represented in pixel or voxel can be applied to the FE model and analyzed as patient-specific material properties under patient-appropriate loading conditions.

The set of data acquired from the uncorrupted image on the number of pixels and distribution of grey-level values from pixel intensity or each voxel in the 3D image can be converted to bone mineral density values in mg/mm^3 or $gram/cm^3$. At the time of generating an intensity histogram for a 2D radiographic image alongside pixel quantities and pixel intensities, the calculated density values can be depicted on the z-axis. This combined set of data when represented on x, y, and z coordinates is termed here as the *intensity-density histogram* (Fig. 2). Thus, the standard 2 coordinate intensity histogram is converted into 3 coordinate histograms presenting grey-scale values on the x-axis, the number of pixels on the y-axis and calculated tissue density on the z-axis. The process of tissue density measurement because of x-ray beam attenuation, whether hard or soft tissues, is one of the salient features of the hyalite sol-gel HSG-Amoeba model to extract information from the distribution of the grey-level value of each pixel/voxel of a segmented image at the time of apoptosis of the model. From the distribution of tissue densities in the segmented R-O-I, the distribution of elastic modulus can be derived for finite element modeling and analysis of the anatomical structure objectively in a virtual environment to elucidate patient-specific quantification under patient-appropriate conditions.

The remainder of the article describes the structure of Amoeba Proteus and its biophysical properties, various phases, and algorithm scheme for the clinical application of the HSG-Amoeba model. The goal is to explore the application of the HSG-Amoeba model for modeling the thoracic skeleton, illustrated here on the sternum, and finite element analysis to carry out an n-of-1 trial, the subject of a future study, to choose an ameliorative implant for the reconstruction of the sternum following open-heart surgery.

4.0 Functional structure of Amoeba Proteus

Amoeba Proteus is a single-celled eukaryote (having a nucleus) freshwater living organism. It has a completely self-sustaining organization in its protoplasm enclosed in a membrane to carry out metabolic processes and motility (Fig. 3). The heterogeneous protoplasm has outer ectoplasm and inner endoplasm containing all the essential elements. The encapsulated protoplasm with its organelles also helps create and preserve shape during motion. It is the flow of sol-gel nature of the protoplasm that effectively implements forward propagation powered by the assembly of actin filaments in the pseudopodium(Pollard & Borisy, 2003; Verkhovsky et al., 1999).

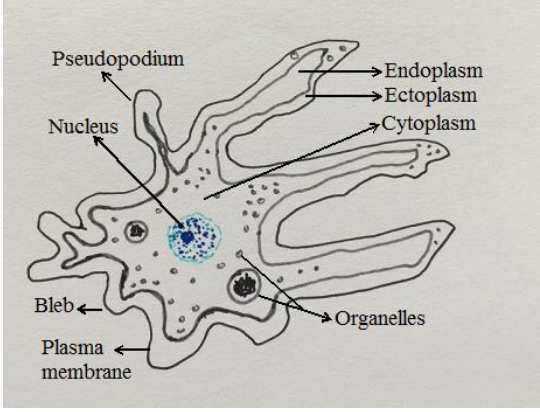

Figure 3 – The basic structure of the Amoeba proteus.

The pseudopodium of the amoeba has a tubular cross-section with a rounded apex. These structures are formed instantaneously by the coordinated action of microfilaments present in the endoplasm pushing out the plasma membrane in the form of a projection, changing its shape rapidly to propel and advance towards the intended direction. The endoplasm is granular, and the ectoplasm contains Actin filaments, which motorize the organism to its target destination. The rapid adaptability of the organism to the environment, its versatile motility, and

the fate of the protoplasm at the time of its natural death (apoptosis) is the main physical characteristics that have been included in the design of the HSG-Amoeba model.

The three-dimensional structure of the Amoeba can throw out multiple temporary projections of pseudopodia to actuate and progressively promote directional movements determining its speed and trajectory(van Haastert, 2011). Generally, the motile cells in animals respond to directional chemical, electrical and thermal signals for orientation to move forward(Bahat & Eisenbach, 2006; Weiner, 2002; Zhao, 2009). The training of these cells on a variety of signals tends to modulate the trajectory of their pseudopodia. During movement in search for potential targets in the environment the spatial-temporal properties of the cells help extend these protrusions further. When there are multiple potential targets to forage the periphery of a large field as the source of directional signals the organism can generate as many new pseudopodia as necessary to effectively perform the search all around. Such a characteristic capability makes Amoeba robust and persistent in its search to cover a large area following the shortest path in the shortest time. This distinctiveness confers Amoeba to start several new pseudopodia all around to match the number of signaling targets facing it. The pseudopodia are formed normal to the membrane surface and by changing position the protrusion is biased to develop a trajectory towards a specific signal.

4.1 Sol-gel oscillating theory and function of Actin-myosin assembly

A synthetic polymeric material undergoes self-oscillation under constant conditions without any off-on switch triggered by external stimuli(Onoda et al., 2017). The synthetic self-oscillating gels were designed by utilizing the Belousov-Zhabotinsky reaction(Tyson, 1994) that results in periodic reduction-oxidation changes and the emergence of spontaneous spatial-temporal patterns. In these kinds of self-oscillating gels, an object can be autonomously transported in a tubular self-oscillating gel by a peristaltic pumping motion. The viscosity oscillation amplitude of 2000 mPa is equal to the oscillation amplitude in the living amoeba(Onoda et al., 2015). It is well known from the network of percolation theory that the elastic modulus is proportional to density and the number of cross-linking points in space. Rheological properties of the sol-gel cytosol are such that at the final stage the HSG-Amoeba model attains stable sequential aggregation forming a solid-state based on percolation theory.

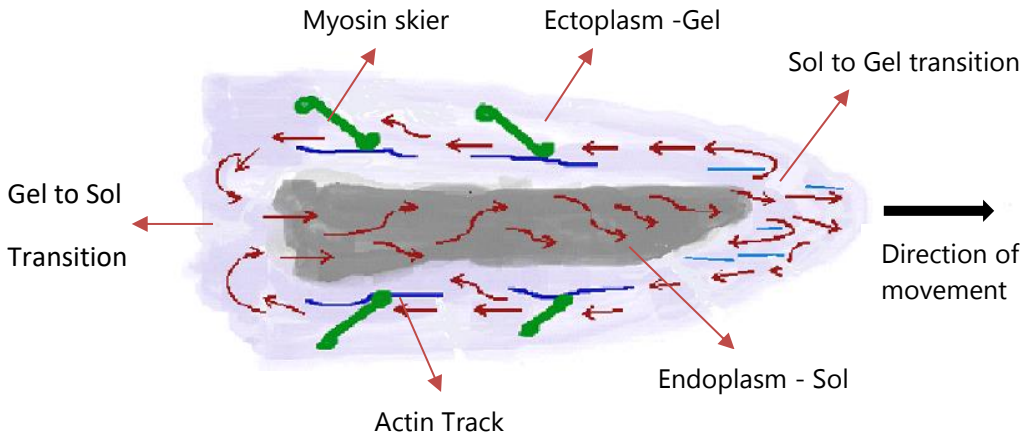

Figure 4 – Pseudopodium showing mechanism of Amoebic movement based on sol-gel theory. The Amoeba "drags" forward with the coupling of the Actin-myosin, pawl-rachet mechanism, during the sol state of the cytoplasm (Artwork in MS Paint).

In the Amoeba, the sol of the endoplasm moves in the traveling direction and transforms to a gel state at the apex of the pseudopodia (Figs. 4). The gel in the ectoplasm transforms into sol to replenish the existing sol state of the endoplasm. This periodic sol-gel conversion is responsible for its movement. Hydrostatic pressure generated in the cell is caused by the contraction of the actin-myosin present in the ectoplasm layer. The flow occurs as the actin-myosin relaxes. The membrane potential of the Amoeba is known to have polarity inside and outside it, which likely controls and refines the direction of its movements(Bingley, 1966).

Actin-myosin contraction in the 2D lamellipodium generates a centripetal action flow – powering the contraction, which results in a spatially graded flow. Actin growth at the boundary results in protrusion to counter retraction, and the balance between protrusion and retraction shapes the lamellipodium. It is this 2D model of actin-myosin mechanisms that reproduce steady-state shapes and speed, as well as self-polarization of a motile cell(Wolgemuth et al., 2011), whereas the dynamic model(Slepchenko & Loew, 2010; Wolgemuth et al., 2011) of Actin-myosin is an algorithm for modeling cell motility in realistic cell geometries.

5.0 Physiology and physics of HSG-Amoeba model

The physiology of the biophysical HSG-Amoeba model is governed by the principles of solid and fluid mechanics, bioelectricity, and biotransformation of protoplasm. It is founded on the assumption that Amoeba is a mass of protoplasm surrounded by a robust elastic membrane to be an independent entity, containing cytoskeleton assembly of actin-myosin with the ability to couple mechanically to generate forward motion(Blanchoin et al., 2014) and permanently decouple at termination. The flow of sol-gel protoplasm based on fluid mechanics assists in the motion and preservation of its shape. The endoplasm is made up of less viscous fluid sol and ectoplasm with its actin-myosin organelles is a highly viscous gel component (Fig. 4). The contraction and retraction of the gelatinous sol-gel extend the pseudopodium, and the resulting flow of the sol drives the gel towards the apex of the pseudopodium(Onoda et al., 2017). Mechanically, the heterogeneous gelatinous protoplasm along with a load of its organelles possessing viscoelastic properties(Marella & Udaykumar, 2004) is powered by the pawl-ratchet type coupling-decoupling mechanism of Actin-myosin to advance the pseudopodium forward (Fig. 5). These biological and mechanical processes collectively form the basis to empower the HSG-Amoeba model to generate motion of the organism by developing interaction with its substrate like that of a motile cell(Coskun & Coskun, 2011).

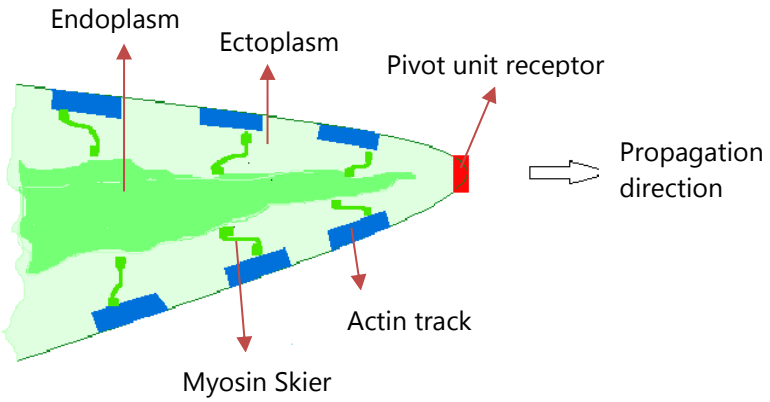

Figure 5 – Structure of apical end of a pseudopodium (Artwork in MS Paint).

Like the biomechanical tactics by which the Amoeba Proteus swims across the fluid medium, the HSG-Amoeba model glides its way into the *substrate* formed by the medium of an image for segmentation according to its intensity gradient and texture (*substrate-intensity*). The attraction and gliding propagation of the model under the influence of image intensity gradient is termed *intensiotaxis*. Actin-myosin interaction generates force within the apical end of the pseudopodium for forwarding motility of the protrusion. Each time the pseudopodium elongates it displaces the apical facet carrying the *pivot unit receptor* (*apex receptor*) possessing a heightened positive electric charge towards the nearest *edge pixel receptor* having a matching heightened negative charge. The formation of the pseudopodium begins with the contraction of the enclosing membrane by the initiation of the actin-myosin system in the ectoplasm to squeeze the protoplasm. An increase in the hydrostatic pressure within it generates a spherical bleb formation that extends into a protrusion(Yoshida & Soldati, 2006), activating the function of sol-gel viscous fluid to form a pseudopodium obeying sol-gel physical theory.

The self-organizing structure of pseudopodia of the HSG-Amoeba model learns progressively to forage and search their targets along the edges of an R-O-I. They are intrinsically controlled and respond to the external *intensiotaxis* signals arising out of the image substrate and edge targets that trigger the formation of new pseudopodia depending on the number of future trajectories to match the number of *edge pixel receptors*. In

the case of segmenting a structure like ribs, irregular posterior elements of thoracic vertebrae, and deep concavities the model is designed to form oblate- and prolate-shaped signal-based directional pseudopodia. The pseudopodia may appear one by one like spreading a network from post to post or at the same time overwhelming the R-O-I at once. This behaviour of the model will be entirely dependent on the design of the algorithm. The diffusion speed of the pseudopodia(Bosgraaf & van Haastert, 2010) advancement is relative to the image intensity gradient and drag caused by its texture. The viscoelastic hydrotonic action of the sol-gel medium provides smooth non-jerky motility for the stability of pseudopodium and its apex. The overshooting and undershooting activity of the pseudopodia is controlled by electrical polarity and charge differential between the apex pivot receptors, the edge pixel receptors, and the opposite charge at the boundary contour separating the adjacent regions.

During propagation, the model will experience drag force according to Newton's third law and Reynolds's number(Bosgraaf & van Haastert, 2010). The drag is induced by image heterogeneity and intensity gradient forming the substrate intensity, as well as the number and shape of the pseudopodia. At the time of its termination as the apical pivot unit receptor of the pseudopodia smoothly docks on to the edge pixel receptor all the mechanical and local bioelectric forces are decoupled. It is the shape and size of the R-O-I and the signals that trigger the structural evolution of the HSG-Amoeba model to segment the R-O-I.

During image processing to segment the R-O-I the model essentially undergoes six phases _

1) A single mother-Amoeba undergoes asexual division to form multiple HSG-Amoeba daughters depending on the number of regions for segmentation.

2) Seeding of HSG-Amoeba models, one in each region of interest.

3) Development and formation of pseudopodia for each HSG-Amoeba model.

4) Intensiotaxis propagation by gliding process into image matrix foraging through 2D/3D space of the image substrate to search for edges based on intensity gradient (pixel grey-level values) and distribution of matching electrical charge within the R-O-I.

5) Termination of propagation at the edge receptors and edge-line pixels, and

6) Apoptosis of the model with phase transformation of its sol-gel protoplasm condensation into solid-state acquiring 2D/3D anatomy of the segmented region.

6.0 Functional principles of the HSG-Amoeba model

The kinetics and kinematics of the HSG-Amoeba model are defined under the term *intensiokinesis*. The process of *intensiokinesis* is based on an image intensity gradient providing kinetic energy for *intensiotaxis* to generate stimulus-response activity and the kinematics (motility) of the model. The HSG-Amoeba model interacts in an invasive and time-dependent fashion within the field of interest for the segmentation of a hosting image. The key events are adherence of the apical *pivot unit receptor* at the apex of a pseudopodium to the *pixel receptor* at the edge, followed by the advancement of the *inter-apical receptor zones* of the pseudopodia and the edge-line *inter-receptor edge pixels* to mark the entire edge and termination of all the advancing pseudopodia to ultimately define the edge and boundary contours (Fig. 6). This ability of the model to interact with intensity gradient underpins the success of the segmentation process. The concept of pixel receptors and polarization of the model membrane with respect to the R-O-I have matching opposite charges at the apical *pivot unit receptors* to that of the *edge pixel receptors*, and a similar charge at the boundary contour to prevent overshooting is a key feature in refining segmentation process for its success in surgical applications to achieve pixel-level excision (described elsewhere by the author), for example of a malignant tumour embedded within important structures with minimal access endoscopic surgery.

The HSG-Amoeba is a semi-automatic model and none of its activities are subject to random autonomous stimulation from the heterogeneous distribution of the image intensity gradient unless specified *intensiokinesis* parameters are given by the operator. The velocity of the model migration is parametrized for a steady progression of the pseudopodia across the substrate taking the shortest distance to reach the edge. The motility

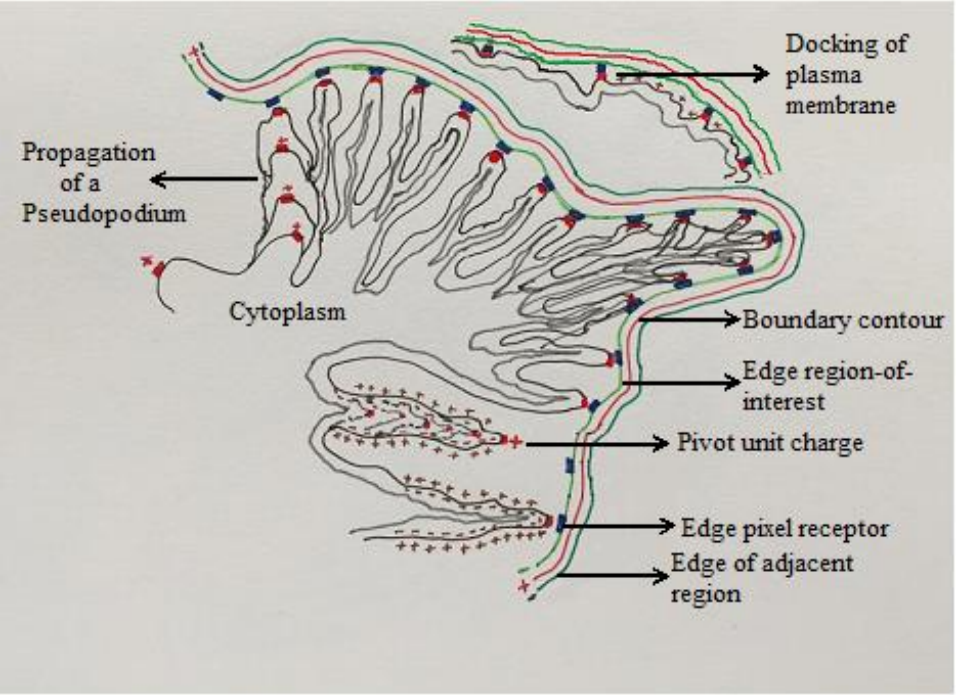

Figure 6 – A detailed illustration showing the formation of multiple pseudopodia, appearance of the blebs, their development into pseudopodia and propagation during segmentation to locate the edge of a region-of-interest; and docking of the apical pivot unit receptor on the edge pixel receptor and intervening HSG-Amoeba membrane on the inter-receptor edge pixels marking out single-pixel width edge contour.

parameters can be assigned in each new instance depending on the size and shape of R-O-I, substrate intensity gradient, random noise, and field electrical charges set to substrate viscosity and drag that influences the motility of pseudopodia. The model can be trained to pace its motility smoothly during its propagation from zero initial velocity to zero termination velocity by proportionately altering the elasticity and rigidity of its membrane, hydrokinetics of cytoplasmic sol-gel viscosity, the electric charge distribution of the image substrate to change drag due to image viscosity. The activity of the entire model comes to a halt automatically at the completion of the segmentation process and it undergoes apoptosis with biotransformation of its protoplasm equilibrating to match heterogeneous image intensity gradient and texture to represent varied tissue density.

7.0 Biotransformation feasibility of the HSG-Amoeba model

The process of phase transition is a complete transformation of a substance from one physical state to an entirely new state possessing new physical properties in the presence of specific factors. The same has been applied to the HSG-Amoeba model for the conversion of the sol-gel and organelles in its protoplasm to translate heterogeneous tissue intensities to equivalent tissue densities. The contents of the model first transform into translucent and then into an opaque solid-state to match the intensity gradient and texture *(substrate-intensity gradient)* of the image matter. The diverse pixel grey-level values thus converted to material densities are used for extracting material properties of the native tissues.

In physical chemistry, each substance is known to have three phases into which known substances can be changed back and forth(Olander, 2019). There are six types of physical processes by which a substance can experience phase transition such as melting, freezing, evaporation, condensation, sublimation, and deposition. All these phases may not be entirely applicable to the protoplasm of the HSG-Amoeba model and its transition into image intensity gradient and texture properties. The normal biological tissue can undergo a phase change from solid to liquid due to necrosis, and from liquid to solid-state in the form of coagulation of blood and tissue proteins; and liquefaction of necrosed tissue to pus and cheese-like consistency called caseation, depending upon the type of acute or chronic bacterial infection, altering physical state of the biological substances. The tissues represented in almost all the medical images are a combination of solid and fluid phases without any empty spaces. This is true in the case of chest radiographic images where there is a large volume of air in the

lungs and blood in the vascular system. Pathological images such as cysts, abscesses, and very soft friable malignant tumours, generally solid, can have relatively greater quantities of liquid phase or loose and sparse tissue texture. It is the proportion of a specific substance phase that decides the image intensity gradient and texture. This is well recognized as variable image intensity observed in MRI T1 and T2 (relaxation time) weighted image sequences, which is not at all like x-ray beam attenuation. For example, the cerebrospinal fluid in a T1 image appears dark grey, fat is bright, and in a T2 image CSF appears brighter, and fat is light grey. The intensity levels displayed and described as grey-level pixels are arranged in a matrix produced because of radio frequency information contained in the signal by conversion to shades of grey after Fourier transformation. Therefore, the image *substrate-intensity* gradient in an MRI image does not represent variable tissue densities as in the case of CT and conventional x-ray images. Apart from the structural arrangement of tissue elements and overall structural geometry which provide structural strength, it is the distribution of specific tissue density that represents the intensity gradient of a conventional x-ray image.

8.0 Operations of HSG-Amoeba model

The sol-gel protoplasm represented in the model evolves from a translucent colourless medium into a thick opaque material called hyalite, like the formation of opal. Hence the name of the model is *hyalite sol-gel Amoeba*. The model operates on the principles of biomechanics, bioelectric, hydrokinetic forces, and biotransformation for phase changes under the influence of external image intensity gradient producing *intensiotaxis* signals and *intensiokinesis*. The objective of the model is to segment a 3D radiographic image constructed from 2D multiple radiographic views into solid-state anatomy at the time of its apoptosis in a quantifiable manner. Ultimately to extract tissue densities and elastic modulus to create a 3D FE model for numerical analysis of patient-specific tissues, with or without implants, under patient-appropriate loading conditions.

Within each extensile pseudopodium, the embedded actin-myosin complex in the gel medium of the ectoplasm of the HSG-Amoeba model mediates gliding motion and experiences viscous drag relative to the image intensity gradient acting as its substrate. The smoothness and regularity of its entire membrane are maintained by the equilibrium between the sol-gel thrust and actin-myosin activity and electrical potential distributed inside and outside the membrane of the pseudopodia. The surfaces of the enclosing membrane of the model have a negative charge inside and a positive charge outside. The single layer of edge pixels representing the R-O-I has a negative charge and the boundary contour pixels outside the edge pixels have a positive charge to prevent overshooting of the moving front of the model. The single file of the pixels making the edges is provided with *pixel edge receptors* at regular intervals to attract *pivot unit receptors* at the apical facet of the pseudopodia to increase the precision of the segmentation process. The pixels forming the edge and boundary contour are assigned the charges after applying an efficient edge detection algorithm such as a thresholding, the Canny edge detector(Canny, 1986) or done manually.

The HSG-Amoeba model does not come with artificial intelligence to act autonomously. It is an interactive model with the learning ability to perform segmentation of a specific anatomical region unless programmed for universal application. Where an image such as a chest radiograph for segmentation has multiple components, the mother Amoeba model undergoes a suitable number of divisions.

Functionally, each of the daughter HSG-Amoeba models is a complete entity and evolves independently to its final state of apoptosis. The *pivot unit receptors* on the apex of the pseudopodia locate and adhere to the *edge pixel receptors* one by one in tandem and terminate by charge neutralization. The model membrane follows the theory of elasticity when given appropriate parameters to shrink or extend and smooth out at the edge to uniformly mark the edge pixels in between the *edge pixel receptors* by charge neutralization as well. The positively charged outer surface of the model membrane is prevented from overshooting the edge by repelling positive charges at the boundary contour. The same bioelectric phenomenon applies when the model membrane meets an acute concave edge. The model membrane prolates to form a sharp pseudopodium and follows the electrical field gradient to enter the concave edges rather than jump across it. The strength of the bioelectric phenomenon overrides any noise-related flaws in the region-of-interest. The R-O-I may be divided into pre-receptor, receptor, and post-receptor pixel zones to define the body, edge, and boundary contour respectively.

At the apical facet of the progressing pseudopodium, the guiding *pivot unit receptor* carries a strong positive electric charge relative to the lower positive charge on the rest of the outer surface of the membrane, so that except for the apex receptor no other part of the membrane adheres on to the matching negative charge of the *edge pixel receptors*. The differential potential of the membrane and similar charges on its extrinsic surface prevents the formation of ruffles and entanglement of the pseudopodia respectively that may otherwise reduce the precision of segmentation. The greater the number of negative *edge pixel receptors* greater will be the precision to define the edge. For a large R-O-I with concavities and irregular edges, the number of pseudopodia can be hundreds in the case where a tumour on the luminal surface of the intestine is for segmentation.

The structure of the actin-myosin complex is laid and aligned in the form of a skier on a track to assist controlled growth and motion of the pseudopodia (Fig. 5). The myosin acts like a skier and new actin tracks are laid each time the pseudopodia grow in length. The myosin filaments ski over the track formed by the actin with their oar-like processes akin to the ratchet-pawl mechanism. The myosin filaments couple and decouples with newly formed actin tracks along with the forward flow of the sol-gel in the endoplasm-ectoplasm complex extending the pseudopodia forward in search of the nearest *edge pixel receptor*. The actin-myosin activity in the ectoplasm in conjunction with sol-gel currents within the pseudopodium directed by *intensiotaxis* carries with it the model membrane forward. This iterative growth of the pseudopodium and trailing membrane continues until the *pivot unit receptor* at its apex meets the nearest *edge pixel receptor* to terminate its propagation.

The motility of pseudopodia and spread of the HSG-Amoeba model across the R-O-I is iterative and time-dependent. As almost all the medical images representing normal or pathological anatomy are heterogeneous, non-spherical, and irregular it is not practically feasible to expect the model pseudopodia propagating at the same velocity to reach the entire perimeter of the R-O-I at the same time. Therefore, it will be only appropriate that the designed algorithm provides a lateral sweeping front to the advancing pseudopodia such that *pivot unit receptors* forage and search for nearest *edge pixel receptors* in tandem rather than randomly collide with each other. However, a collision between the pseudopodia is prevented by the anti-collision and anti-crowding effect due to repelling forces of similar surface charges as an important bioelectric parameter of the model.

The termination of the pseudopodium automatically inhibits the actin-myosin coupling through an inhibitory feedback mechanism. The whole process is iterative and repeated until all *edge pixel receptors* are blocked. After the adhesion of the apical *pivot unit receptors* of two adjacent pseudopodia is tethered to the adjoining *edge pixel receptors*, then the inter-receptor segment of the membrane between the pseudopodia is directed to propagate until it is smooth following the elastic theory to terminate at the edge pixels in-between *inter-edge pixel receptors* by charge neutralization. The free membrane front takes the shortest path by including any of the known algorithms (Dijiskstra algorithm, Hamilton-Jacobi equation, nearest neighbor algorithm, repetitive nearest neighbor algorithm) to reach the edge pixels. It also effectively enhances the process of the *pivot unit receptor* on the apex of the pseudopodium to search for the nearest negatively charged *edge pixels receptors*. The noise distribution of specific pixel intensity within the R-O-I is given an appropriate positive charge to repel the moving membrane front to skip it like a well-adapted living organism to overcome an obstruction in its path.

9.0 Application of the Hyalite sol-gel Amoeba model

The biomimetic deformable HSG-Amoeba model operates under the influence of biophysical processes in conjunction with bioelectric membrane potentials and electrical charges implemented on image substrate, edge, and boundary pixels. The model is applied after the completion of the preliminary step of the edge detection process to the R-O-I in an image. For optimal edge detection, a combination of Canny and Sobel edge techniques is preferred to yield a single-pixel width edge and to remove weak edge pixels respectively. Then HSG-Amoeba model is introduced to complete segmentation of the entire three-dimensional R-O-I. The organism glides and deforms multiple times to diffuse in the image substrate encompassing the entire symmetric or asymmetric R-O-I to acquire its morphology by redefining edge and boundary contour from the adjacent regions.

The framework of design and function of the HSG-Amoeba model is theoretically exemplified here on the sternum (Fig. 7); however, it can be extended to the articulating clavicles, bony ribs, costal cartilages, and thoracic vertebrae. The exercise is primarily directed at the reconstruction of the osteochondrotomy of the sternum

following open-heart surgery. Whenever possible the whole thoracic cage with the inclusion of functioning articulations, muscles, and ligaments, as well as breasts in females should be reflected during modeling and numerical analysis for surgical applications to truly make the assessment patient-specific and patient-appropriate as an n-of-1 trial study. All the tissue parameters and numbers for application must originate from a given patient under consideration rather than assumed or experimentally determined generic values available in the literature.

An intact sternum is a central binding component that helps maintain the dynamic shape of the elastic thoracic skeleton as it moves in coronal and sagittal planes simultaneously to alter the volume and correspondingly the shape of the thoracic cavity with each breath. The sternum experiences significant variable stresses and strain because of physiological and pathological loads applied to any of its parts and at each costal level with change

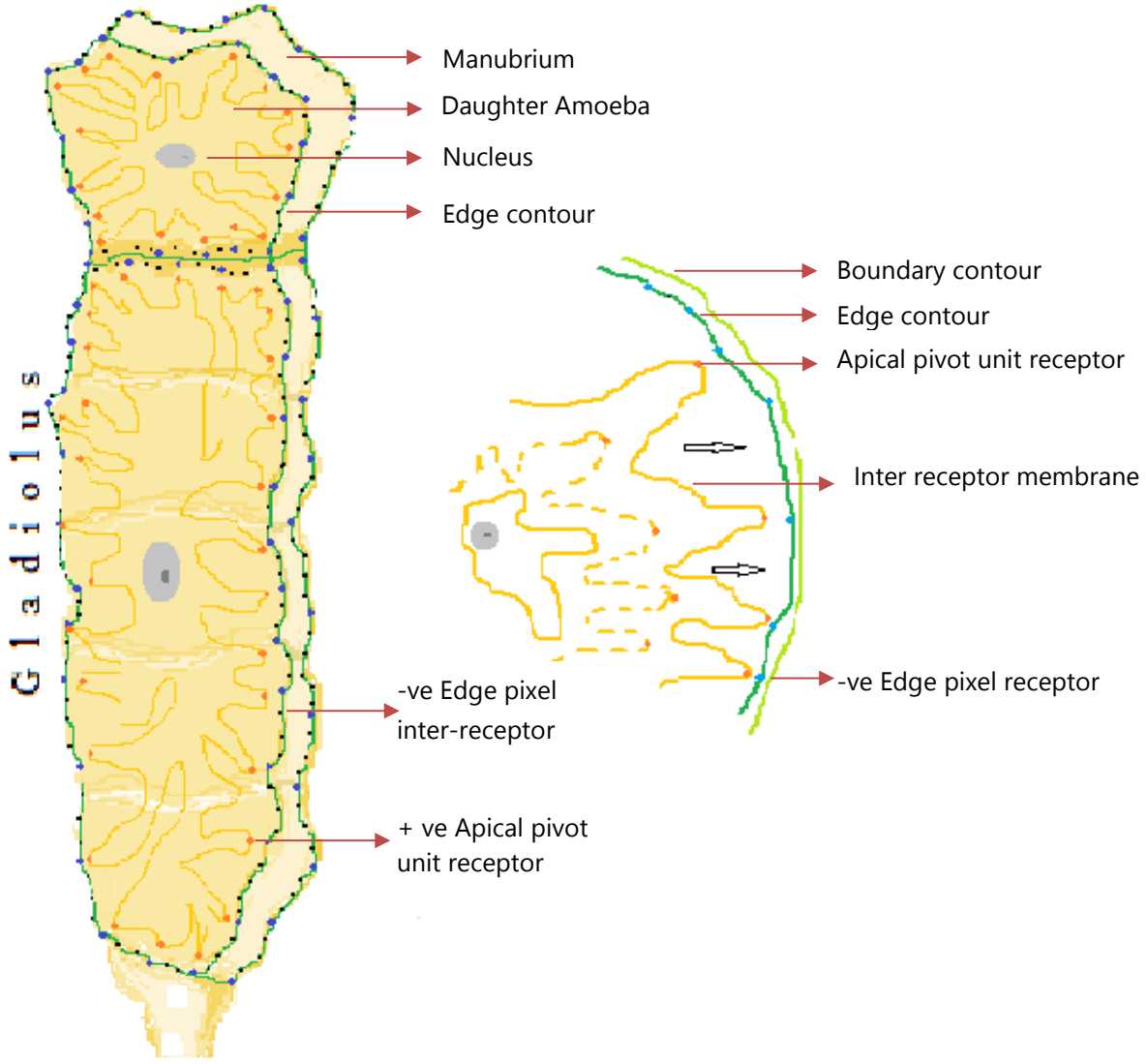

Figure 7 – In detail display of two independent daughters Hyalite Sol-Gel Amoeba model operations in the manubrium and gladiolus sections of the sternum: segmentation process in progress (Art in MS Paint).

in sagittal and coronal diameters and axial plane act on it simultaneously. Therefore, the decision taken arbitrarily to only includes the affected anatomy for numerical analysis provides less than reliable information for surgical application on the belief that observed differences in the results of experimental modeling and clinical outcome are statistically insignificant. Although a limited approach for cost saving is acceptable for research purposes in an engineering laboratory for higher education but unacceptable to carry out surgical intervention when it will be neither patient-specific nor patient-appropriate for higher analysis. The possibility of failure due to a time-dependent cumulative effect is a real event.

The steps in the evolution of the HSG-Amoeba model during the image segmentation process are as follows_

9.1 Asexual reproduction of Amoeba Proteus

The division of mother-Amoeba into daughter-Amoebae depends on the number of R-O-I for segmentation and advanced image analysis. To include all the thoracic cage elements the mother-Amoeba divides into 32 daughter-Amoebae to seed one sternum, ten pairs of right and left ribs including costal cartilages, and upper eleven of the twelve thoracic vertebrae. Mother-Amoeba divides into two and the asexual division continues to further produce 32 daughter-Amoebae, altogether up to five generations ($2^5 = 32$). In the event only one R-O-I requires segmentation then only the mother-Amoeba model would be sufficient. The mother Amoeba may be kept in reserve where the regions-of-interest are odd in number or more regions need to be included in the study as the thoracic cage is part of the axial skeleton, and the abdominal wall plays an important role in the biomechanics of the thorax.

9.2 Seeding HSG-Amoeba model and establishing edge pixel charges

Each of the 32 daughter Amoebae is either placed automatically or interactively in an already constructed 3D model of the thoracic skeleton. The daughter-Amoebae can distribute automatically in the image based on the threshold range selected from the pixel-intensity histogram. The pixel layer outside the edge pixels is labeled as boundary pixels. The edge pixels of each of the skeletal elements are given a negative electrical charge and the labeled boundary contour pixels receive a positive charge. For precision, many edge pixels are given heightened negative charge to act as *edge receptor pixels* matching heightened positive charge on *pivot unit receptor* on each pseudopodium of the daughter Amoebae. The arbitrarily chosen interval of fifteen to twenty pixels between two adjacent heightened negatively charged *edge receptor pixels* may vary depending on the size of the region for segmentation and complexity of the edges, the ability of the central processing unit of the computer, software design, and the necessity to speed up the process.

9.3 Formation and development of pseudopodia

Once each of the daughter Amoebae is in its respective thoracic skeletal element, edge pixels and boundary contour pixels have been given the appropriate charges, the Amoeba membrane blebs to initiate the formation of pseudopodia. The number of pseudopodia depends upon the size, geometry, and the number of heightened negative charge *edge receptor pixels*. The apex of each pseudopodium receives an equivalent heightened positive charge and the membrane in between them receives uniform positive charges on the outside and negative charges on the inside of the model. When the apical heightened positively charged apex reaches the nearest heightened negative charge receptor of the edge pixel layer there is charge neutralization as soon as the apex docks onto the edge pixel receptor terminating the motion of the apex. The positively charged extrinsic surface of the membrane in between the two apices advances, if needed shrinks or stretches, and smooths out to remove redundancies to match and meet the edge parameters in between the *edge pixel receptors*.

9.4 Propagation of pseudopodia and phenomenon of intensiotaxis

The propagation of the pseudopodia relies on several mechanisms to speed-up smooth advancement towards the edge pixel layer. The image pixels forming the substrate based on their grey-level values (intensity gradient) are given matching negative electrical charge gradients all over the domain for movement of the apical *pivot unit receptors* of pseudopodia and to help negotiate shallow and deep narrow concavities of the boundary contour lined by the edge pixel layer. The fixed nominal and heightened positive charges on the membrane and apex of pseudopodia respectively follow the negative charge distributed across the substrate and positive charge to repel noise intensities to prevent obstruction and premature docking of pseudopodia.

The substrate negative gradient varies based on the distribution of grey-level pixel intensities due to varying tissue densities. The magnitude of pixel grey-level values carrying equivalent electrical gradients at each point provides the required image energy. With an image of 8 integers at each pixel with a grey-level range of 0-255, there will be a significant difference in gradient magnitude even if the range, to say, between the pixels is125 and 225. A matching gradient scale is developed for the negative charge across the whole substrate to generate *intensiotaxis* (attraction due to pixel intensity variations) between the model and image substrate. The apical charge on the leading end of pseudopodia locates the closest neighbouring pixels of a higher gradient from

one of the three pixels ahead of it like pawns of a chessboard (Fig. 8). In 3D R-O-I apical *pivot unit receptor* of pseudopodia forage pixels in all the three coordinates to make the next move. And, where pixel intensities and

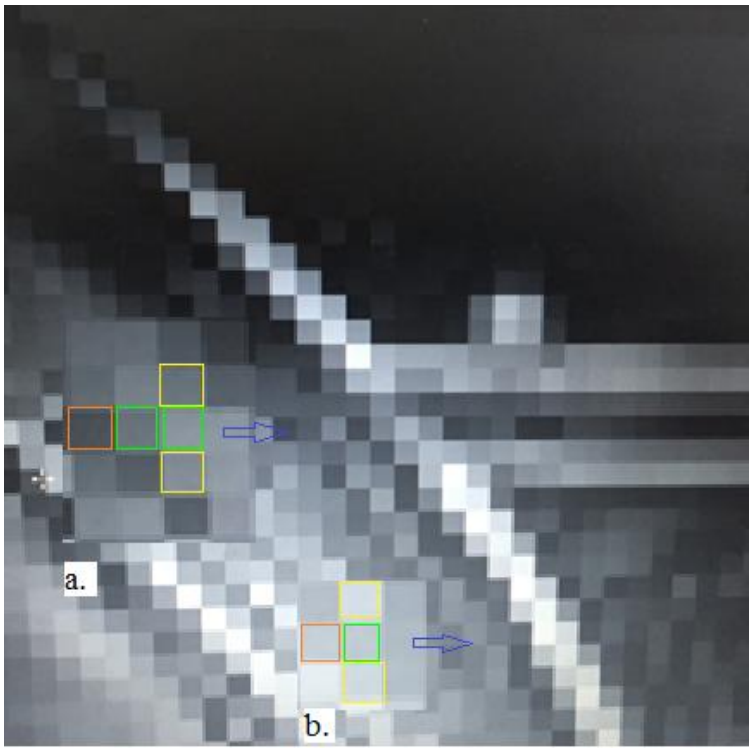

Figure 8 – Suggested chess board a. knight b. pawn movements of the HSG-Amoeba model. Green boxes suggest forward movements and yellow optional diagonal movements, and blue arrow direction of progression.

the electrical gradient is homogeneous, to speed up the segmentation process pseudopodia may be made to move like knights by developing a three-dimensional chess system. At each new pixel station, the apex provides feedback to the actin-myosin complex to couple, motorizing the *pivot unit receptor* to move forward. On reaching the next station it decouples and receives a fresh message to get ready to couple again. Instead of random mass movements, it has a choice of limited movements like a pawn and a knight to steer the apex of the pseudopodia forward to prevent drifting of the *pivot unit receptor*.

If a pseudopodium does drift, then similar extrinsic charges on its surface will repel to prevent collision between the adjacent pseudopodia and to help put it back on its original track to forage territory only ahead of it. The energy to move is computed for the same number of neighbourhood pixels each time, preferably focused at the most applicable pixel intensity and negative charge gradient magnitude at each iteration. The amount of nominal negative charge on the edge pixel layer is decided by the edge pixel intensities and the heightened negative charge of the *edge pixel receptors* is given a matching heightened positive charge of the apical *pivot unit receptor* to achieve charge neutralization. The stimulus-response algorithm matching the bioelectrical charges and intensity gradient bioluminescence mechanisms are synchronized with biomechanical actin-myosin contraction and relaxation to ensure uniform-sized steps and smooth motion of the model.

The 3D pseudopodia of the model glide forward by translating and dilating through a three-dimensional substrate to cover the virtual space of the image like an Amoeba Proteus in the real-world domain to engage in substrate medium to forage in all directions. The model body is designed to remain anchored at a suitable point of initialization from where it throws out the pseudopodia to drive the apices forward at each iteration process. There is coupling-decoupling feedback to the actin-myosin complex at each iteration assisted by other mechanisms. If the selected interval between the *edge pixel receptors* is large and there is too much of the redundant intervening membrane, though unable to tangle due to similar extrinsic charges on the membrane surface, an additional step of excision and splicing can be included. In the same way, supplementary length or

surface may be added. The apex with a heightened positive charge may be adjusted to overcome the faltering action due to noise intensities in the image and speed up the process.

9.5 Termination of propagation at the edge pixels

The termination criterion is based on opposite electrical charges resulting in 'charge neutralization'. The *pivot unit receptor* at the apex of each pseudopodium upon meeting the *edge pixel receptor* with equivalent heightened charge terminates the propagation of pseudopodia and the in-between membrane smooths out to meet the *inter-receptor edge pixels* to complete part segmentation of R-O-I. The overshooting of the pseudopodia and in-between membrane is prevented by the repelling force of the positive charges on the boundary contour pixels. The same happens if multiple adjacent regions of interest are being processed at the same time by other daughter-Amoebae at the articulations of the ribs with the sternum and vertebrae. The same would be applicable if the costal cartilages are managed separately from the bony ribs.

9.6 Apoptosis of the Amoeba Proteus model and biotransformation

The HSG-Amoeba model structure does not disappear from the image substrate at the end of the segmentation process as it deforms to encompass the whole 3D image space, filling the entire anatomy subjected to the model. Instead, the apoptosis of the HSG-Amoeba model akin to the natural death of Amoeba Proteus is represented as phase transformation of sol-gel protoplasm condensation into a solid-state appearing like hyalite. Once the membrane of the HSG-Amoeba model has been transfigured to the shape of three-dimensional regional anatomy the protoplasm and the organelles of the model meld into the substrate and transform to attain the original image intensities of every pixel within the image domain. As a result, the model acquires 3D anatomy of the thoracic skeletal elements and at the same time tissue densities equivalent to pixel intensities as numerical grey-level values representing x-ray beam attenuation. If the amount of beam energy attenuation is known, then tissue density can be calculated from it as the higher the density higher will be the beam energy attenuation. The biological residue of the biomimetic model adaptively metamorphoses to elucidate tissue densities and ultimately material properties can be extracted for the development of a patient-specific thoracic skeleton finite element model and patient-appropriate analysis.

Given the model expectations, the whole process from the initial step of edge detection to the final numerical outcome of the voxel-based finite element mesh will be the best without changing the computer space. It would require advanced computer facilities such as a graphic processing unit for parallel processing of the data. When multiple implants are compared to select the most ameliorative implant design, then multiple computing stations in parallel are run to provide all the results within the same time frame.

10.0 Framework of HSG-Amoeba Algorithm for clinical application

As described in the literature, primarily the mathematical algorithm employed for active contour translation is based on variational calculus to achieve energy minimization at the termination of the model curve to mark the edges and run on internal and external energy parameters(Kass et al., 1988). To refine the original "Snakes" active model curve, the algorithm was upgraded based on dynamic programming which can move a given number of control points on the curve across a given number of neighbourhood pixels at each iteration process(Amini et al., 1990). To overcome deficiencies in the "Snakes" to delineate concavities intelligent inflating balloon and gradient vector force models(Duan & Qin, 2001; Xu & Prince, 1997) were introduced. However, each design came with individual advantages and disadvantages.

The main objective of an algorithm is to help all the control points on a deformable curve model to converge on the edge effectively segmenting the R-O-I. The HSG-Amoeba was conceived to build and exploit a model which has a continuous closed curve with a maximum number of control points like a rosary for a 2D image space or a closed 3D structure with the ability to expand casting into 3D anatomic space. And, have highly directed sensitive points to forage a three-dimensional image space with a maximum number of control points on its surface to match the multifarious geometry of the boundary contour. It is a fact that none of the medical images are homogeneous and without artifacts. The perturbing noise generated by perpetual electromagnetic photons and electronics of an imaging system is hard to eliminate. To overcome such inadvertent manifestations that corrupt image quality and to preserve the original pixel grey-level values representing the tissue properties

the HSG-Amoeba model has multiple mechanisms to harvest meaningful and clinically applicable information for patient management. In surgical practice there is a danger of failure of surgical treatment when parameters are based on results of ex-vivo biomechanical experiments on limited size tissue samples and destructive techniques, statistically averaged results for finite element analysis based on numerous assumptions.

A digital medical image presented for analysis is not a continuous function of spatial variables. It is a discrete function of integers within spatial coordinates. As a result, the algorithms are only approximations, analogous to the real-world coordinate derivative representing the original spatially continuous image, which is an analogue image based on physical quantities rather than numerical code. In a digital image, the edge is represented by high-intensity discontinuities and a steep intensity gradient to distinguish the R-O-I from the adjacent regions. The R-O-I is made up of pixels of similar values clustered together only if the region has a similar type of tissue density and edges have relatively higher intensity pixels unless occluded by a distinctively different adjacent structure. However, for the sake of explanation, if the R-O-I has similar pixel properties, then to find the edges the model pseudopodia and membrane will span the image gradient and converge to mark the edges where the pixels have the highest intensity. In such a case the relationship between various bioactive energy mechanisms of the HSG-Amoeba is_

$M(a) = [x(a), y(a)]^t$, where M is the HSG-Amoeba membrane representing the model curve and a is the model. If E is total system energy and E' is one of the sub-energies of various system components, then

$E_{(HSG\text{-}Amoeba)} = E'_{1\ (actin\text{-}myosin)}$ [intrinsic mechanical action (a)] + $E'_{2\ (image)}$ [extrinsic gradient magnitude of the pixel intensities as pixel negative charge (a)] + $E'_{3\ (electrical\ charges)}$ [apex (a)] + $E'_{4\ (electrical\ charges)}$ [membrane(s)] ds

$E'_{1\ (actin\text{-}myosin)}$ = (Pseudopodium elastically expanding and stretching) + (Intervening membrane shrinking and smoothing)

$E'_{2\ (image\ substrate\ intensity)} = E'_{2\ (pixel\ negative\ charge)}$

Termination 'Charge Neutralization' = E'_{5+6} (edge pixel receptor negative charge + other in-between edge pixel negative charges) - E'_{3+4} (apex pivot unit receptor positive charge + membrane positive charges] = 0

Anti-collision E'_7 = (membrane to membrane repelling positive charges)

Anti-ruffle E'_8 = (membrane intrinsic negative and extrinsic positive charge differential to prevent ruffle formation)

10.1 Algorithm steps

The algorithm begins once a 3D virtual thoracic skeletal image is ready and can be animated to visualize all its parts.

Input image: The original unmodified 3D stereo-radiographic or 3D reconstructed image of the thoracic skeleton using other imaging modalities such as CT.

Output image: The final output image is the one that is obtained after the computing process ends following the phase transformation of the HSG-Amoeba model to deliver material properties, ready for numerical analysis.

To define a single layer of edge pixels and boundary contour pixels apply thresholding Canny edge detection and Sobel operator or any of the advanced edge detection algorithm such as the convolutional networks can also be used to perform a preliminary image segmentation process. Following this_

Step 1: Bioelectric negative charge is given to all the detected edge pixels and heightened negative charge to *edge receptor pixels* demarcated at selected regular intervals. Similarly, the boundary contour pixel layer just external to the edge pixel layer is given a positive charge

Step 2: The mother-HSG-Amoeba undergoes asexual division to generate 32 daughter-Amoebae

Step 3: Each of the daughter Amoeba is seeded within 32 skeletal elements of the thoracic cage, preferably initialized approximately in the centre of each domain, not that it is necessary

Step 4: The HSG-Amoebic membrane is given intrinsic negative and extrinsic positive differential charges to prevent collision between pseudopodia and the ruffling of the membrane. The algorithm proceeds to develop the required number of micro blebs and each of the blebs due to become pseudopodium is given a heightened positive charge at the *pivot unit receptors* relative to the heightened negative charge at the *edge pixel receptors* of the domain

Step 5: According to the intensity gradient the pixel grey-level values distributed in the region-of-interest are given a negative charge of equivalent magnitude and establish a feedback mechanism for the actin-myosin complex to couple-decouple the advancing apex of the pseudopodia

Step 6: The mechanism of the Actin-myosin complex is arranged in x, y and z axii like a skier on corresponding tracks in each coordinate. The provided energy moves mace-shaped paddles of the myosin (the skiers) on the actin surface (the tracks) through the electrical coupling-decoupling process (contraction and relaxation) to advance the apex of the pseudopodia

Step 7: Membrane excision, addition, and splicing processes to remove redundancies

Step 8: Smoothing elastic shrinking and stretching of the membrane after latching of the *pivot unit receptors* to two adjacent *edge pixel receptor* sites

Step 9: Iterative advancement of the pseudopodium apex follows chessboard pawn or knight movements following the increasing pixel intensity of the substrate and to overcome noise intensities without getting stuck mid-stream before reaching the true edge

Step 10: The heightened positive charge *pivot unit receptor* of the pseudopodium docks on to the heightened negative charge of the *edge pixel receptor* at regular intervals and terminate its motion upon convergence to reach a charge neutralization state; and repel from the positive charges of the boundary contour pixels to block overshooting

Step 11: The intervening membrane length measure up to match the length or surface area of the edge proportionately to converge and reach charge neutralization to terminate the motion and block overshooting

After the completion of the configuration of the HSG-Amoeba model to match the 3D anatomy of R-O-I follows_

Step 12: Phase transition of protoplasm and included organelles in the endoplasm and ectoplasm of the HSG-Amoeba model transform its biological material to match the original pixel grey-level intensities of the image substrate representing the native tissue densities recorded at the time of imaging of the real-world anatomy and preserved during stereo-radiography to reconstruct a 3D virtual model

Step 13: Conversion of in-situ patient-specific tissue densities to elastic modulus at every pixel of the image which is now a true representation of the original three-dimensional anatomy and physiological material properties of the thoracic skeleton. At this stage, it is optional to return the subtracted soft tissues of the thoracic model and complete the model with articular cartilage, ligaments, capsules, and external musculature, and in a female subject breast volume and mass is hung on to the modeled skeletal anatomy

Step 14: The prepared 3D thoracic cage virtual model is converted to a voxel-based FE mesh model for the application of patient-appropriate boundary conditions at all the thoracic skeletal elements, articulations, musculature, and breasts where appropriate

Step 15: For an n-of-1 trial to proceed, on a 3D thoracic skeletal model perform mid-sagittal osteochondrotomy of the sternum and for its reconstruction, a selection of already prepared implant models is set in place before applying boundary conditions, and the force equivalent to three times the patient-appropriate loads. Depending upon the number of implant designs selected for comparison on a particular patient set in place the same number of thoracic models to run in parallel on separate computers simultaneously

Step 16: Once the numerical analysis is complete and the data is available, the process reaches its end to deliver patient-specific and patient-appropriate information for surgical application.

Then most responsible and painstaking process for a clinical biomechanical engineer begins when it is time to analyze and understand the collected information to confidently discuss with the operating surgeon why to

recommend a particular implant design for a given patient. At the same time, the surgeon's experience must be taken into consideration before the patient is provided with information to sign a well-informed consent for selecting the most ameliorative implant design to reconstruct osteochondrotomy of the sternum at the time of wound closure in the upcoming surgery.

11.0 Comments and conclusion

Historically, there had been numerous segmentation and registration techniques based on energy minimization and active contour along with the development of algorithms based on level-set principles to successfully evolve the curve to help overcome changing topography of the image(Gandhi, 2022). Unlike industrial and leisure activity images, medical images are heterogeneous with a significant number of instrument-related artifacts and noise. During analog to digital image processing to improve contrast and smooth the image features for presentation many projected characteristics and original properties of real-world objects are either altered or lost. This kind of image processing also alters original tissue densities as a function of x-ray beam attenuation. It means there is a loss of important parameters for the extraction of representative mechanical properties acquired from tissue densities by applying one of the prevalent power laws, even though these laws are less than optimum. Thus, the available methods fall short in their accuracy for clinical application and surgical management. All this tends to reduce the reliability and reproducibility of the numerical results for sincere recommendations as to the standard of patient care. These are some of the main reasons that such techniques have not successfully entered daily surgical practice. Despite the huge success of computer vision and artificial intelligence in industry and virtual imagery in motion pictures.

More recently, the focus has been on the rapid development and expansion of deep learning techniques such as convolutional neural networks (CNN) with much greater acceptance. CNN and machine learning are extremely good when focused on the segmentation of a wide variety of tumour tissues and diagnosis, with their pros and cons when it comes to clinical applications(Aggarwal et al., 2021; Peng & Wang, 2021). Like the old well-known algorithms, the newer algorithms have been largely used for processing medical images including segmentation and 3D reconstruction of CT images, and for planning radiotherapy treatments where there is no need for clinical application of tissue material properties. There are only a few known but less used methods to extract tissue densities from averaged pixel intensities as HU. However, the literature does not provide reliable means to extract the material properties of tissues in question as there are huge variations in methodology, particularly the power laws for the conversion of densities to the elastic modulus for higher numerical analysis.

The main objective of conceiving the biomimetic hyalite sol-gel Amoeba model is to undertake various steps from edge detection through encompassing three-dimensional segmentation of applicable regions to finally procure *patient-specific* and *patient-appropriate* numerical values without alteration of original characteristics and tissue properties represented in the image. At the same time, the endeavour is to complete the whole process in a continuous fashion within the same computer space from beginning to end.

The reason to choose Amoeba Proteus as the archetypical model design is because of its shape-changing versatility and physiology. It also fits well into the longstanding philosophy of physics-based active curves. The attractive property of the asexual division of Amoeba Proteus has been incorporated into the HSG-Amoeba model to assist easy dispersion and seeding of multiple sites within a busy multilayered image of variegated tissue densities reflected as pixel intensities for utilization at higher-level analysis and surgical applications. The phenomenon of pseudopodium to prolate and advance during motion, forage the environment, and enter deep narrow crevices naturally is well suited to the need of medical image processing at special anatomic sites such as elongated structure of costal cartilages and ribs, vertebral transverse and spinous processes, and extremely irregular edges forming narrow and sharp deep concavities in a malignant tumour. The bioactive physiology-based mechanisms are more intuitive in contrast to many physics-based rich algorithms, difficult to comprehend fully for mathematically less gifted physicians interested to learn the role of computer vision in medical image processing. In this respect, the need for a program and the role of the clinical biomechanical engineering team have already been discussed elsewhere(Gandhi, 2022).

The major limitation of the article is the lack of much-needed rigours of a mathematical algorithm to demonstrate the worthiness of the HSG-Amoeba. Even though mathematical algorithms provide

approximations of the real world, they are still important for patient care and fail-proof surgical applications. The finite-element modeling and numerical analysis based on engineering principles are the only means to prove the effectiveness of new mechanical concepts. The focus of the study was to present the design and framework of the conceived HSG-Amoeba model, introduction to basic science principles of computer vision, and optical density to relate it to the central theme of procuring tissue densities. Interested physicians need to become acquainted with imaging modalities how to acquire a 3D model of R-O-I, the role of volume rendering 3D Sonography, and revisit stereo-radiography techniques. Its role in *patient-specific* and *patient-appropriate* surgical applications to select the most ameliorative implant based on an n-of-1 trial has been considered in one of the following studies of this series. It is expected that in due time the worthiness of the HSG-Amoeba model and the suggested biomimetic framework of the model would be advanced further for clinical research to interest the medical community in collaboration with a dedicated in-house clinical biomechanical engineering team.

Conflict of interest: The author declares that he has no conflicts of interest.

Funding: The study was unfunded.

References

Aggarwal, R., Sounderajah, V., Martin, G., Ting, D. S. W., Karthikesalingam, A., King, D., Ashrafian, H., & Darzi, A. (2021). Diagnostic accuracy of deep learning in medical imaging: a systematic review and meta-analysis. In *npj Digital Medicine* (Vol. 4, Issue 1). Nature Research. https://doi.org/10.1038/s41746-021-00438-z

Amini, A. A., Weymouth, T. E., & Jain, R. C. (1990). Using Dynamic Programming for Solving Variational Problems in Vision. *IEEE Transactions on Pattern Analysis and Machine Intelligence*. https://doi.org/10.1109/34.57681

Bahat, A., & Eisenbach, M. (2006). Sperm thermotaxis. *Molecular and Cellular Endocrinology*. https://doi.org/10.1016/j.mce.2006.03.027

Bannur, S. V., Kulgod, S. V., Metkar, S. S., Mahajan, S. K., & Sainis, J. K. (1999). Protein determination by ponceau S using digital color image analysis of protein spots on nitrocellulose membranes. *Analytical Biochemistry*. https://doi.org/10.1006/abio.1998.3020

Bingley, M. S. (1966). Membrane potentials in Amoeba proteus. *Journal of Experimental Biology*.

Blanchoin, L., Boujemaa-Paterski, R., Sykes, C., & Plastino, J. (2014). Actin dynamics, architecture, and mechanics in cell motility. *Physiological Reviews*. https://doi.org/10.1152/physrev.00018.2013

Bosgraaf, L., & van Haastert, P. J. M. (2010). Quimp3, an automated pseudopod-tracking algorithm. *Cell Adhesion and Migration*. https://doi.org/10.4161/cam.4.1.9953

Buckle, C. E., Udawatta, V., & Straus, C. M. (2013). Now you see it, now you don't: Visual illusions in radiology. *Radiographics*. https://doi.org/10.1148/rg.337125204

Canny, J. (1986). A Computational Approach to Edge Detection. *IEEE Transactions on Pattern Analysis and Machine Intelligence*. https://doi.org/10.1109/TPAMI.1986.4767851

Coskun, H., & Coskun, H. (2011). Cell Physician: Reading Cell Motion A Mathematical Diagnostic Technique Through Analysis of Single Cell Motion. *Bulletin of Mathematical Biology*. https://doi.org/10.1007/s11538-010-9580-x

Dolz, J., Desrosiers, C., & Ben Ayed, I. (2018). 3D fully convolutional networks for subcortical segmentation in MRI: A large-scale study. In *NeuroImage*. https://doi.org/10.1016/j.neuroimage.2017.04.039

Duan, Y., & Qin, H. (2001). Intelligent Balloon: A subdivision-based deformable model for surface reconstruction of arbitrary topology. *Proceedings of the Symposium on Solid Modeling and Applications*.

Gandhi, H. S. (2019). Rationale and options for choosing an optimal closure technique for primary midsagittal osteochondrotomy of the sternum. Part 3: Technical decision making based on the practice of

patient-appropriate medicine. *Critical Reviews in Biomedical Engineering*. https://doi.org/10.1615/CritRevBiomedEng.2019026454

Gandhi, H. S. (2022). A Comprehensive Review of Computer Vision Techniques to Interest Physicians and Surgeons, Role of A Clinical Biomechanical Engineer in Pre-Operative Surgical Planning, And Preamble To HSG-Amoeba, A New Concept of Biomedical Image Modeling Technique. *International Journal of Computers and Technology*, *Vol. 22 (2022)*, 1–49. https://doi.org/10.24297/ijct.v22i.9219

GEOFF DOUGHERTY. (2009). *Digital Image Processing for Medical Applications*. Cambridge University Press.

Haralick, RM. & Shapiro, L. (1985). Image Segmentation techniques. *COMPUTER VISION, GRAPHICS, AND IMAGE PROCESSING*, *29*, 100–132.

Jones, N. (2014). Computer science: The learning machines. In *Nature*. https://doi.org/10.1038/505146a

Kass, M., Witkin, A., & Terzopoulos, D. (1988). Snakes: Active contour models. *International Journal of Computer Vision*. https://doi.org/10.1007/BF00133570

Marella, S. V., & Udaykumar, H. S. (2004). Computational analysis of the deformability of leukocytes modeled with viscous and elastic structural components. *Physics of Fluids*. https://doi.org/10.1063/1.1629691

Olander, D. R. (2019). *General Thermodynamics* (1st ed.). Boca Raton : CRC Press.

Onoda, M., Ueki, T., Shibayama, M., & Yoshida, R. (2015). Multiblock copolymers exhibiting spatio-temporal structure with autonomous viscosity oscillation. *Scientific Reports*. https://doi.org/10.1038/srep15792

Onoda, M., Ueki, T., Tamate, R., Shibayama, M., & Yoshida, R. (2017). Amoeba-like self-oscillating polymeric fluids with autonomous sol-gel transition. *Nature Communications*. https://doi.org/10.1038/ncomms15862

Peng, J., & Wang, Y. (2021). *Medical Image Segmentation with Limited Supervision: A Review of Deep Network Models*. http://arxiv.org/abs/2103.00429

Pollard, T. D., & Borisy, G. G. (2003). Cellular motility driven by assembly and disassembly of actin filaments. In *Cell*. https://doi.org/10.1016/S0092-8674(03)00120-X

Saito, S., Yamashita, T., & Aoki, Y. (2016). Multiple object extraction from aerial imagery with convolutional neural networks. *IS and T International Symposium on Electronic Imaging Science and Technology*. https://doi.org/10.2352/ISSN.2470-1173.2016.10.ROBVIS-392

Slepchenko, B. M., & Loew, L. M. (2010). Use of Virtual Cell in Studies of Cellular Dynamics. In *International Review of Cell and Molecular Biology*. https://doi.org/10.1016/S1937-6448(10)83001-1

Swaroop, P., & Sharma, N. (2016). An Overview of Various Template Matching Methodologies in Image Processing. *International Journal of Computer Applications*. https://doi.org/10.5120/ijca2016912165

Tyson, J. J. (1994). *What Everyone Should Know About the Belousov-Zhabotinsky Reaction*. https://doi.org/10.1007/978-3-642-50124-1_33

van Haastert, P. J. M. (2011). Amoeboid cells use protrusions for walking, gliding and swimming. *PLoS ONE*. https://doi.org/10.1371/journal.pone.0027532

Verkhovsky, A. B., Svitkina, T. M., & Borisy, G. G. (1999). Self-polarization and directional motility of cytoplasm. *Current Biology*. https://doi.org/10.1016/S0960-9822(99)80042-6

Wang, Q., Lin, J., & Yuan, Y. (2016). Salient Band Selection for Hyperspectral Image Classification via Manifold Ranking. *IEEE Transactions on Neural Networks and Learning Systems*. https://doi.org/10.1109/TNNLS.2015.2477537

Weiner, O. D. (2002). Regulation of cell polarity during eukaryotic chemotaxis: The chemotactic compass. In *Current Opinion in Cell Biology*. https://doi.org/10.1016/S0955-0674(02)00310-1

Wolgemuth, C. W., Stajic, J., & Mogilner, A. (2011). Redundant mechanisms for stable cell locomotion revealed by minimal models. *Biophysical Journal*. https://doi.org/10.1016/j.bpj.2011.06.032

Xu, C., & Prince, J. L. (1997). Gradient vector flow: A new external force for snakes. *Proceedings of the IEEE Computer Society Conference on Computer Vision and Pattern Recognition*.

Yoshida, K., & Soldati, T. (2006). Dissection of amoeboid movement into two mechanically distinct modes. *Journal of Cell Science*. https://doi.org/10.1242/jcs.03152

Zhao, M. (2009). Electrical fields in wound healing-An overriding signal that directs cell migration. In *Seminars in Cell and Developmental Biology*. https://doi.org/10.1016/j.semcdb.2008.12.009